Thermal conductivity of biobased insulation building materials measured by hot disk: Possibilities and recommendation

T. Colinart, M. Pajeot, T. Vinceslas, A. Hellouin de Menibus, T. Lecompte

▶ **To cite this version:**

T. Colinart, M. Pajeot, T. Vinceslas, A. Hellouin de Menibus, T. Lecompte. Thermal conductivity of biobased insulation building materials measured by hot disk: Possibilities and recommendation. Journal of Building Engineering, 2021, 43, pp.102858. ⟨10.1016/j.jobe.2021.102858⟩. ⟨hal-03383286⟩

HAL Id: hal-03383286

https://hal.science/hal-03383286v1

Submitted on 2 Aug 2023

HAL is a multi-disciplinary open access archive for the deposit and dissemination of scientific research documents, whether they are published or not. The documents may come from teaching and research institutions in France or abroad, or from public or private research centers.

L'archive ouverte pluridisciplinaire **HAL**, est destinée au dépôt et à la diffusion de documents scientifiques de niveau recherche, publiés ou non, émanant des établissements d'enseignement et de recherche français ou étrangers, des laboratoires publics ou privés.

Distributed under a Creative Commons CC BY-NC 4.0 - Attribution - Non-commercial use - International License

Version of Record: https://www.sciencedirect.com/science/article/pii/S2352710221007166
Manuscript_9db92595595c32107aa802fdbd16fbca

Thermal conductivity of biobased insulation building materials measured by hot disk: possibilities and recommendation

T. COLINART[1*], M. PAJEOT[1], T. VINCESLAS[2], A. HELLOUIN De MENIBUS[3,4], T. LECOMPTE[1]

[1] Univ. Bretagne Sud, UMR CNRS 6027, IRDL, F-56100 Lorient, France

[2] UniLaSalle, 3 rue du tronquet, 76134 Mont-Saint-Aignan, France

[3] Eco-Pertica, Hôtel Buissonnet, 61340 Perche-en-Nocé, France

[4] Association Nationale Des Chanvriers en Circuits Courts, 79500 Melle, France

Corresponding author:

Thibaut COLINART

IRDL – Université de Bretagne Sud

Rue de saint Maudé, BP 92116,

56321 Lorient Cedex, France

Phone: 33/0 2 97 87 45 17

Fax: 33/0 2 97 87 45 72

Mail : thibaut.colinart@univ-ubs.fr

© 2021 published by Elsevier. This manuscript is made available under the CC BY NC user license
https://creativecommons.org/licenses/by-nc/4.0/

Abstract

The Hot Disk transient plane source (TPS) method allows characterizing the thermal properties of various materials in a few minutes. Particularly, it is increasingly used for evaluating thermal conductivity of insulation building materials. However, the results of such measurement frequently differ from steady state measurements because of the significance of heat transfer into the Hot Disk sensor. Even if improvements have been proposed for specific cases, they cannot be generalized, especially for heterogeneous materials like biobased building insulation materials. The objective of this study is to evaluate all previously evaluated sources of errors when conducting a measurement with current capabilities of Hot Disk commercial device. Three types of material are tested: conventional isotropic materials (like XPS), compressible anisotropic materials (like wood fiber insulation) and heterogeneous anisotropic materials (like light-earth biobased concrete). The influence of setting parameters (volumetric heat capacity, temporal bound for estimation) is analyzed in light of repeatability and reproducibility errors. The suitability of hot disk method based on isotropic or anisotropic model to characterize non-transverse isotropic heterogeneous materials is discussed and compared with steady state measurements.

Keywords

Thermal conductivity; Hot Disk; Biobased material; Light-earth biobased concrete; Wood fiber insulation; Anisotropic material;

1 Introduction

In the building sector, external wall thermal insulation is one of the most important issue to improve energy efficiency and to reduce greenhouse gases emissions. Nowadays, a variety of building insulation materials are either commercialized or under development [1-4]. For all materials, the accurate knowledge of thermal properties is extremely important, since it is used in building performance simulation and it determines some subsidy. Overview of current experimental methods for evaluating thermal properties can be found in [5]. Steady-state methods, such as Heat Flow Meter or Guarded Hot Plate, are accurate techniques when conducted carefully. Therefore, they are rather well adapted to measure thermal conductivity of insulation materials [6]. However, they require large sample size and experiments may take a long time in view of reaching thermal equilibrium or hygrothermal equilibrium in case of moist sample. To shorten the experiments, transient methods were developed. Among them, the transient plane source technique, commonly referred as the Hot Disk method, was designed to estimate thermal diffusivity α and thermal conductivity λ of isotropic homogeneous solid materials [7]. According to the standard 22007-2 [8], the thermal properties can be estimated over a wide range ($5 \times 10^{-8} < \alpha < 10^{-4}$ $m^2.s^{-1}$ and $0.01 < \lambda < 500$ $W.m^{-1}.K^{-1}$) with an accuracy of 5 % for λ and of 10 % for α [9]. In case of insulation materials, this accuracy is however questioned. Indeed, while a few works observed a good agreement with steady-state methods [10,11], numerous studies noted that thermal conductivity of dry materials can be overestimated by 20 to 50 % [12-18]. Several reasons are proposed to explain these differences: uncertainty in the experimental data and data analysis procedure [19,20] and deviation of theoretical model associated to the set-up [15,18,21-24]. Particularly, neglecting the finite size of the sensor and, thus, its thermal inertia and thermal resistance, seems to be a strong assumption when measuring thermal conductivity of insulation materials [15,18, 23-25]. Coquard et al. [15] suggested that estimated thermal conductivity may deviate from the exact value when thermal

inertia of tested material is too different from the ones of the sensor. Zhang et al. [23] showed that it could be caused by the large heat loss proportion through sensor side. Last, a detailed analysis performed by Zheng et al. [18] confirmed that errors are mainly correlated with the radial heat diffusion and loss in the insulation layer of the sensor, but also with the deviation of temperature distribution in the insulation layer from the ideal case near its interface with the sample. Interestingly, they proposed an error map as function of thermal conductivity and thermal capacity for one sensor type, simplified through a convenient polynomial correction function. Besides, other heat transfer modes like radiation [15], convection [18] or latent heat transfer [10] are expected to have limited influence on the results obtained with Hot Disk. Note, however, that these analyses prevail mainly for isotropic materials. Some extensions are proposed for orthotropic materials which are evaluated with an anisotropic model [25,26]. Unfortunately, not all thermal insulation building materials are isotropic or orthotropic and some of them are heterogeneous at centimeter scale. This is particularly true for some biobased materials, like natural fiber insulation [27] or biobased concrete, made of plant aggregate and binder like lime or earth [28][29]. Even if Hot Disk has been previously used for such materials [30-32], measurements are performed with only the capabilities that a commercial Hot Disk Thermal Constants Analyzer can provide in the view of evaluating the influence of some factors (moisture content, temperature, density, etc.). In this work, we aim to raise questions about the methodology for the evaluation of thermal properties of two biobased insulation building materials (wood fiber insulation and light-earth biobased concrete).

2 Materials and methods

2.1 Materials

Fives insulating building materials from the market are tested: polyurethan (PU), extruded polystyrene (XPS), foam glass (FG), autoclaved aerated concrete (AAC) and wood fiber insulation (WFI). The four first materials are conventional and supposed to be isotropic. They are used as reference materials to validate the measurement methodology. The last material is biobased and transversely isotropic. Their thermophysical properties (declared thermal conductivity, measured density and specific heat capacity, thermal diffusivity) are gathered in Table 1. All materials with dimensions 130 x 130 x *th* mm^3 (see Table 1) are tested in dry state after being dried in a ventilated oven at 65 °C [33].

	λ [W.m^{-1}.K^{-1}]	ρ [kg.m^{-3}]	c_p [J.kg^{-1}.K^{-1}]	$\rho\, c_p$ [MJ.m^{-3}.K^{-1}]	α [mm.s^{-1}]	*th* [mm]
PU	0.022	31.4 ± 0.1	1268 ± 48	0.04	0.55	50
XPS	0.029	32.3 ± 0.2	1239 ± 13	0.04	0.72	50
FG	0.036	85.1 ± 1.1	817 ± 6	0.07	0.52	50
AAC	0.150	522.8 ± 1.4	930 ± 8	0.49	0.31	34
WFI	0.038	58.3 ± 0.6	1337 ± 30	0.08	0.49	40

Table 1: Thermophysical properties of tested materials.

Light-earth biobased concrete is also tested. This material is obtained by mixing hemp shiv and earth slip according to the setting procedure defined in [34,35]. Here, numerous samples with density ρ ranging from 250 to 800 kg.m^{-3} are prepared by varying hemp dry mass fraction f_{hemp} and water to binder ratio *W/B* (see Table 1). Their compactness *C* [35], defined as the opposite of open porosity, vary between 12 and 32 %. Two sets of samples with dimensions of 100 x

130 x 130 mm^3 were produced: one to be tested parallel to compaction (P-samples) and one to be tested perpendicular to compaction (T-samples). All light-earth biobased concrete samples are dried in ventilated oven at 40 °C [35] and cut in the smallest dimension into two identical pieces with a diamond disc saw before testing. Figure 1 presents the cut surface of samples P35 and T35. One observes more elongated forms of hemp shiv for sample P35 than for sample T35. As expected, it means that hemp shiv tends to rearrange perpendicularly to compaction direction [36]. Finally, light-earth biobased concrete tends to present transversely isotropic structure, for which P-samples (resp. T-samples) could serve to evaluate through-plane (in-plane) thermal conductivity.

Name	Expected density [$kg.m^{-3}$]	f_{hemp} [%]	W/B [-]	ρ [$kg.m^{-3}$]	C [%]	c_p [$J.kg^{-1}.K^{-1}$]
T25	250	40	2.00	255.8	12.6	1097
P35 / T35	350	34	1.23	305.4	14.5	1074
P35r / T35r	350	45	2.41	309.2	15.6	1117
P45 / T45	450	23	0.87	463.1	20.4	1025
P60 / T60	600	17	0.60	651.7	27.7	1000
P80 / T80	800	13	0.43	755.8	31.2	983

Table 2: Mix ratio and thermophysical properties of light-earth biobased concrete.

Figure 1: Cut surface of samples P35 (left) and T35 (right).

2.2 Methods of thermal characterization

Thermal characterization was carried out by means of three experimental facilities: Hot Disk TPS 1500 (Hot Disk AB, Gothenburg, Sweden), a home-made guarded hot plate [37] and micro-DSC III calorimeter (Setaram, Calluire, France).

Hot Disk TPS 1500

The Hot Disk (HD) relies on the transient plane source method [7] to evaluate simultaneously thermal diffusivity α and thermal conductivity λ as follow. A resistive element (usually a nickel double spiral sensor sealed between two thin sheets of Kapton or mica) is clamped between two identical samples and electrically heated by a step-wise Joules heating during a user defined experiment time. The heat flux diffuses into the sample, causing a general increase in the mean temperature of the sensor over time. This mean temperature increase ΔT is evaluated by recording the change in electrical resistance $R(t)$:

$$\begin{cases} R(t) = R_0\left(1 + a\left(\Delta T(\tau)\right)\right) \\ \tau = \sqrt{t/\theta} \\ \theta = r^2/\alpha \end{cases} \quad (1)$$

where t is the time, R_0 is the initial resistance of the sensor before the transient recording, a is the temperature coefficient of the resistivity, θ is the characteristic time, r is the sensor radius. The mean temperature increase is then analyzed by means of a theoretical model. The main assumptions of the model are: heat transfer occurs by conduction into isotropic materials, sensor is placed in infinite medium, sensor is assimilated to uniformly spaced concentric thin rings of a resistive material, sensor thermal inertia and contact resistance between the sensor and the samples are neglected. Under these assumptions, it comes:

$$\Delta T(\tau) = \frac{P_0}{\pi^{3/2} r \lambda_{HD}} D(\tau) \quad (2)$$

where P_0 is the input heating power, λ_{HD} is the thermal conductivity of the tested material and $D(\tau)$ is a dimensionless time function [7].

In a common commercial software (Hot Disk Thermal Constants Analyzer®), two further points are considered. First, a time correction due to unavoidable hardware and software delays t_c is introduced [8]. This time is generally small compared to experiment's time. Second, the mean temperature increase is decomposed into contributions from the sample ΔT_s and the sensor ΔT_i. The latter is the temperature difference between the heat source and the sample surface facing the sensor due to heat transfer into thin insulating layers of the sensor and thermal contact resistance. Nevertheless, ΔT_i becomes almost constant after a short time [23] and only the contribution of ΔT_s is used to estimate the thermal properties. Practically, the estimation is done as follows in the software: characteristic time θ, and thus thermal diffusivity α, is used as fitting parameter to get the best linear proportionality between $\Delta T_s(\tau)$ and $D(\tau)$ on a given interval [t_1 t_2]. Then, thermal conductivity λ_{HD} is deduced from the slope. If volumetric heat capacity ρc_p is known, only λ_{HD} has to be estimated.

The experimental set-up can also be used to evaluate through-plane and in-plane thermal conductivities of transverse isotropic materials. In this case, Eq. (2) becomes:

$$\Delta T(\tau_r) = \frac{P_0}{\pi^{3/2} r \sqrt{\lambda_z \lambda_r}} D(\tau_r) \tag{3}$$

where λ_z and λ_r are axial and radial thermal conductivities, $\tau_r = \sqrt{t/\theta_r}$ and $\theta_r = r^2/\alpha_r$. Characteristic time θ_r is used as a fitting parameter to estimate α_r and, thus, λ_r once the volumetric heat capacity ρc_p is known. Then, λ_z is deduced from the slope of the curve defined by Eq. (3).

In this work, experiments are performed with kapton sensors with radii of 3.189 mm, 6.403 mm, 9.868 mm, 14.61 mm and 29.4 mm. Whatever the sensor, the input power and the duration of the measurement were selected to meet requirements on probing depth, characteristic time and temperature increase. Repeatability and reproducibility tests are

performed. For repeatability tests, experiments are run 3 times in a row (without removing the samples) with a long relaxation time between each experiment to reach thermal equilibrium again. For reproducibility tests, at least three experiments are performed. Before the measurements, it was verified that there is no temperature drift of the samples. All experiments are performed in the lab under ambient conditions (T = 23 ± 3 °C, rh = 50 ± 10 %) and applied pressure is controlled to ensure good contact between samples and sensor. For hygroscopic samples like WFI and light-earth biobased concrete, samples and sensor are wrapped in plastic bag to prevent moisture exchange with ambient air: mass change was always lower than 0.5 % for all experiments. Analyses of the experiments were based on Eq. (2) for isotropic mode, and on Eq. (3) for anisotropic mode. Last, the accuracy of Hot Disk experimental set-up was verified by testing reference steel samples provided by Hot Disk AB.

Guarded hot plate and DSC calorimeter

Thermal conductivities measured by Hot Disk are compared with those measured on Guarded Hot Plate (GHP) device according to the EN 12664 standard [39]. Here, the same samples are tested at a mean temperature of 23 °C. Further details on the set-up can be found in [35,37]. The specific heat capacity measurements are carried out using a micro-DSC III calorimeter (Setaram, Calluire, France) according to the standard ISO 11357-4 [40]. A minimum mass of 20 mg placed in 1 cm^3 sealed vessels is tested in the temperature range of 5 to 30 °C at 0.2 $°C.min^{-1}$. Results are gathered in Table 1 for dry samples and in Table 2 for light earth biobased concrete. For light earth biobased concrete, a mixing law is used knowing the mass fraction and the specific heat capacity of each constituent [35].

3 Results and discussion

3.1 Isotropic materials

Thermal properties of four isotropic materials (PU, XPS, FG, AAC) are determined by means of at least 230 Hot Disk tests analyzed with the isotropic model (see Eq. 2). The objective of this section is to assess the influence of the main factors and to provide some guidelines to ensure the accuracy of the results.

Setting volumetric heat capacity ρc_p or not?

Basically, volumetric heat capacity ρc_p has to be calculated from estimated thermal diffusivity α and thermal conductivity λ_{HD}. Results obtained for at least 30 tests performed with different sensors on each material are shown in Figure 2 and compared to DSC measurements. Differences up to 14 % are observed on ρc_p between HD and DSC. Furthermore, standard deviation ranges between 6 and 16 % for HD, while it does not exceed 1 % for DSC. In the literature, ρc_p is generally overestimated by HD (+40 % for XPS [15], +12 % for AAC [41]). This is supposed to be due to a difference in material conditioning [41] or to the influence of thermal inertia of the probe on the measurement [15].

If ρc_p is known, it can be used as input. This approach allows estimating only λ_{HD} with accuracy [42]. Indeed, an uncertainty of 1 % on ρc_p induces an uncertainty of 0.16% on λ_{HD}. For the tested materials, setting ρc_p has minor effect on estimated λ_{HD} (difference of 1 % between both approach) and on its precision (same standard deviation). On the other hand, it clearly improves the precision on α: standard deviation is decreased from 11.6 % to 6.1 %. Based on these results, it is therefore recommended to set ρc_p when it is possible.

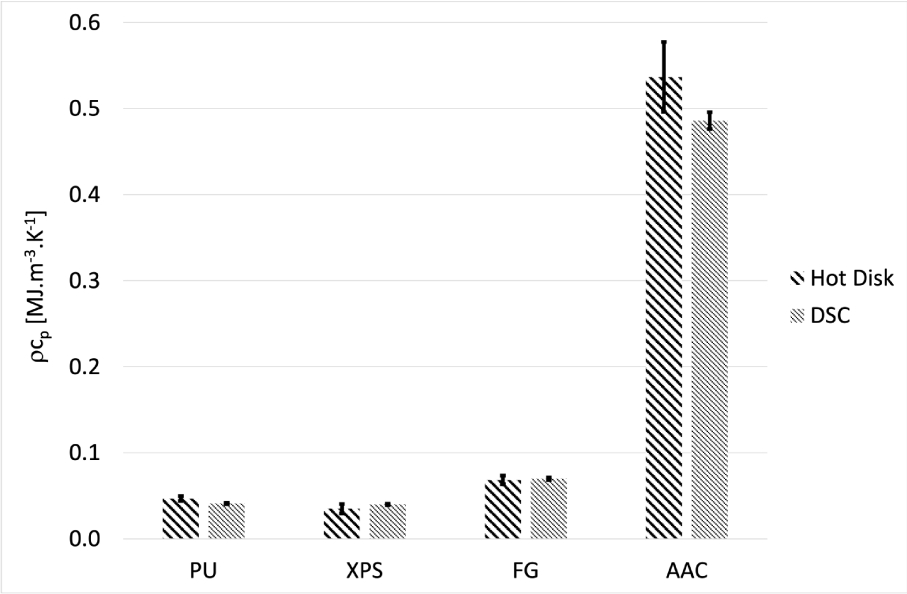

Figure 2: Volumetric heat capacity of various isotropic materials estimated from Hot Disk measurements or measured by DSC.

Influence of bound for estimation

The bound for estimation t_1 and t_2 should be selected so that the residue (*i.e.,* the difference between the measured and simulated temperature) are randomly centered on 0, that a minimum temperature increase is respected, and that penetration depth remains lower than probing depth. Furthermore, it is recommended to remove the first point to avoid any influence of heat diffusion through the sensor [9,18]. From sensitivity analyses [9,21], it is also required that $0.33 < \tau_2^2 < 1$, where $\tau_2^2 = t_2/\theta$. Despite these recommendations, the interval [t_1 t_2] has to be adjusted manually by the user and could have an influence on the estimated values. To evaluate this influence on λ_{HD}, a difference analysis is performed [19] by varying the upper bound τ_2^2 and the interval length. An example of results obtained on PU with sensor 14.61 mm is presented on Figure 3. λ_{HD} tends to decrease with τ_2^2 (which is not necessary the case for other experiments) and converge toward a single value whatever the interval length. More generally, standard deviation ranges between 1 % (PU, FG and AAC) and 4 % (XPS) and the highest difference to an *a priori* estimated value is lower than 3 % (PU, FG and AAC) and 7 % (XPS).

For all the estimations, the residues are well centered on 0 with a slight signature. The highest difference between measured and simulated thermogram is observed close to t_1 (particularly when ΔT_s is higher than 2 K) and confirms the importance of removing the first points in the analysis.

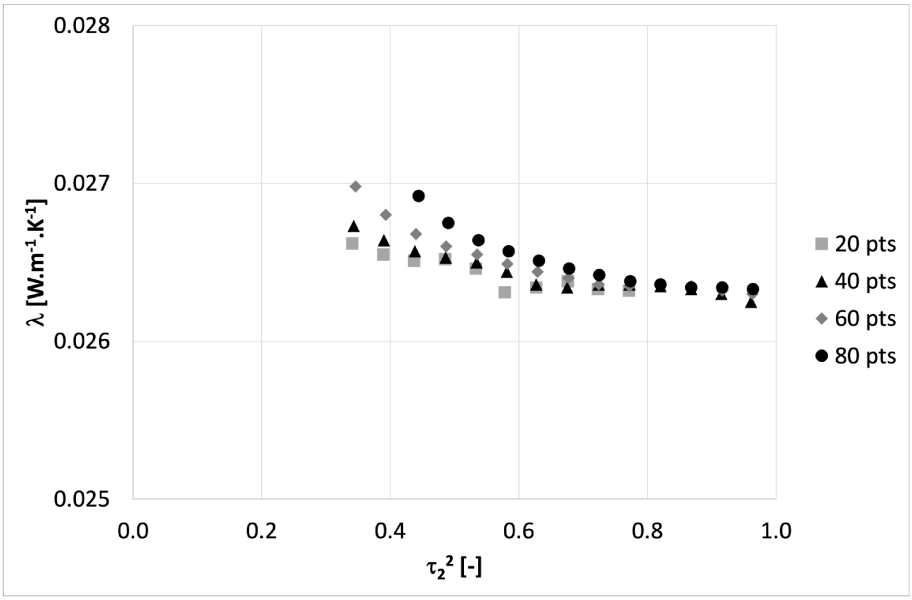

Figure 3: Estimated thermal conductivity λ_{HD} of PU as function of upper bound τ_2^2 and interval length. Measurement is performed with sensor 14.61 mm.

Repeatability and reproducibility of the measurements

Repeatability errors are gathered in Table 3. They do not exceed 4.6 %. The highest error is obtained for the largest sensor. For the sensor 29.4 mm, the analysis was limited since samples dimension could not always ensure that penetration depth is lower than probing depth. Reproducibility is tested for sensors 9.868 and 29.4 mm. While the error does not exceed 3 % for the sensor 9.868 mm, it may reach 9 % for the largest sensor. Such errors seem not due to pressure or temperature. For instance, the applied pressure on the samples was varied between 25 and 250 N on XPS samples without any influence on λ_{HD}. Similarly, even if temperature varied slightly in the lab, no significant trend could be observed on the results. On the contrary,

surface roughness seems to be an influencing parameter. Indeed, XPS samples were cut leading to one smooth and one rough surface. When rough surfaces are tested, λ_{HD} is about 8 % lower than the one measured for smooth surfaces, whatever the sensor radius. A possible explanation relies on the role of contact thermal resistance R_c: the higher R_c, the higher shift in temperature measurement ΔT_i, the lower true temperature variation ΔT_s [21], the higher signal to noise ratio, the less reliable estimation. This point should be further analyzed.

Sensor radius [mm]	**3.189**	**6.403**	**9.868**	**14.61**	**29.4**
PU	0.2 %	0.2 %	0.8 % (2.8 %)	3.2 %	4.6 % (4.9 %)
XPS	0.1 %	0.4 %	3.1 % (2.3 %)	1.0 %	0.8 % (2.7 %)
FG	0.6 %	0.3 %	0.7 % (2.3 %)	2.3 %	3.3 % (7.2 %)
AAC	0.5 %	0.8 %	2.2 % (2.2 %)	1.0 %	1.8 % (8.6 %)

Table 3: Repeatability and reproducibility (in bracket) errors for thermal conductivity λ_{HD} of different materials as function of sensor radius.

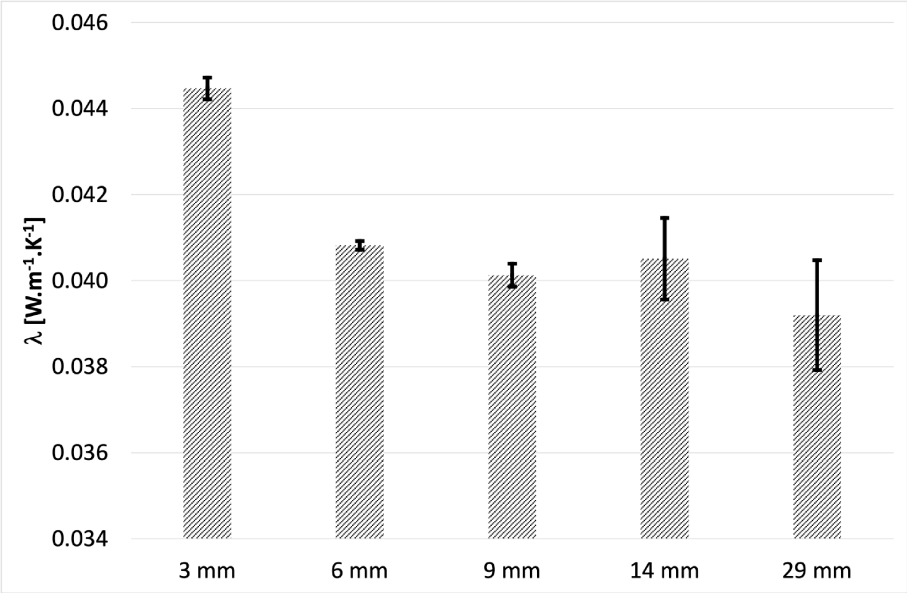

Figure 4: Influence of sensor radius on estimated thermal conductivity λ_{HD} of FG.

Finally, repeatability and reproducibility errors are similar to the uncertainty due to bound for estimation. However, despite good accuracy, results obtained for the smallest sensor radius

differ by 5 to 15 % from other measurements. This point is highlighted in Figure 4 for FG. Trofimov et al. [11] made similar observations and suggested that this is due to heat loss through connecting wire. Besides, residue tends to decrease with increasing sensor radius.

Hot Disk vs Guarded Hot Plate

Considering the low uncertainties on HD measurement, a mean thermal conductivity is calculated for each material from all experiments (except the ones performed with sensor 3.189 mm) and compared to GHP measured value. Results are gathered in Table 4. For isotropic non compressible insulating building materials, a good agreement is found between both methods. Similarly, the maximal difference observed in the literature do not exceed 5% (except for AAC which presents a larger volumetric heat capacity) [41,43-46]. These finding are coherent regarding the error analysis proposed by Zheng et al. [18]: here, thermal diffusivity of tested samples is close to the one of Kapton [15,18,23,25] and, thus, thermal conductivity overestimation should not exceed 5 %. Thermal conductivity of isotropic non compressible insulating building materials can be accurately measured with the HD device.

	Guarded Hot Plate		Hot Disk		Difference	Difference measured in the literature
	Mean	Std-dev.	Mean	Std-dev.		
PU	0.0279	11.5%	0.0269	4.3%	-3.9%	+4.6% [43]
XPS	0.0329	11.6%	0.0328	4.1%	-0.5%	+1 … +4% [44, 15, 11]
FG	0.0390	8.3%	0.0392	5.9%	0.7%	+3% [45]
AAC	0.1478	6.0%	0.1482	5.7%	0.2%	+8 … 13 % [41, 46]
WFI	0.0400	4.2%	0.0504	6.6%	26.1%	

Table 4: Mean thermal conductivity measured on dry insulating materials with Hot Disk and Guarded Hot Plate devices.

3.2 Compressible anisotropic material

Wood fiber insulation (WFI) is an anisotropic and compressible material, in which wood fiber is aligned in a preferential direction on manufacturing plane [47]. Consequently, in-plane and through-plane thermal conductivity are expected to differ. Therefore, the use of an anisotropic model is necessary. For this model, volumetric heat capacity ρc_p is an input. It has no influence on α_r since α_r is estimated directly from the measurement. However, because of the definition of thermal diffusivity and of the linearity of Eq. (3), the uncertainties on λ_z and λ_r are similar to the one of ρc_p while the uncertainty on α_z is doubled. Nevertheless, the reliability of anisotropic model was verified for isotropic non compressible materials: $\lambda_z = \lambda_r = \lambda_{HD}$ within the uncertainty bounds as in [11].

In case of WFI, a further experimental difficulty arises to evaluate density ρ. Indeed, a sufficient pressure should be applied to ensure a good contact between the samples and the sensor. However, because of WFI compressive behavior, sample's thickness (resp. density) decreases (resp. increases) with increasing pressure. Furthermore, the contact may be not so good because of strain relaxation. Nevertheless, despite it could have an influence on repeatability tests, no trend is observed on the results. The repeatability of the measurement is better than 8 % for sensors 6.403 mm, 9.868 mm, 14.61 mm (sensor 29.4 mm is not considered because limitation on infinite medium assumption and sensor 3.189 mm is too small regarding material heterogeneity). Besides, the reproducibility of the measurement done with one sensor size ranges between 2.5 and 16.5 %. Nor surface roughness, nor applied pressure are influencing factors on the accuracy, contrary to bound for estimation. Indeed, a similar analysis as in Section 3.1 reveals that standard deviation on λ_z and λ_r can reach 40 %.

Last, Figure 5 presents averaged values of λ_z and λ_r for all measurements for two values of c_p. First, a value of 1337 J.kg^{-1}.K^{-1} measured by DSC is used (see Table 1). Note that this value is consistent with other experimental data from the literature [48-50]. In this case, $\lambda_z > \lambda_r$ which is in contradiction with expected and previous results on fibrous materials [51-55]. Indeed, the thermal contact between the fiber should cause a lower thermal conduction across the fiber in the z-direction. In the literature, anisotropy ratio ranging between 1.5 and 2 is noted between in-plane and through-plane thermal conductivities. To obtain such ratio for HD measurement, c_p should be increased to increase in-plane thermal conductivity (according to the definition of thermal diffusivity) and to decrease the through-plane thermal conductivity (according to the linearity of Eq. (3)), as underlined by Trofimov et al. [11]. Here, a ratio of 1.64 is calculated when c_p is set to 2100 J.kg^{-1}.K^{-1} (value provided by the manufacturer [56] and available in Wufi database [57]). Furthermore, though-plane thermal conductivity λ_z becomes more consistent with GHP measurement (see Table 4).

To overcome this uncertainty of c_p, it might be interesting to analyze the data with an isotropic model. Results are also plotted on Figure 5. λ_{HD} is estimated with a better accuracy, independently of c_p. However, a value of about 0.5 W.m^{-1}.K^{-1} is found which looks like a mean value between axial and radial thermal conductivities. This value is 25 % larger than the thermal conductivity measured by guarded hot plate (see Table 4), while overestimation ranging between 5 and 10 % is expected from the work of Zheng et al. [18]. Such differences were already observed in the literature [51-52]. Finally, neglecting the transversely isotropic nature of WFI would lead to overestimate the transverse thermal conductivity.

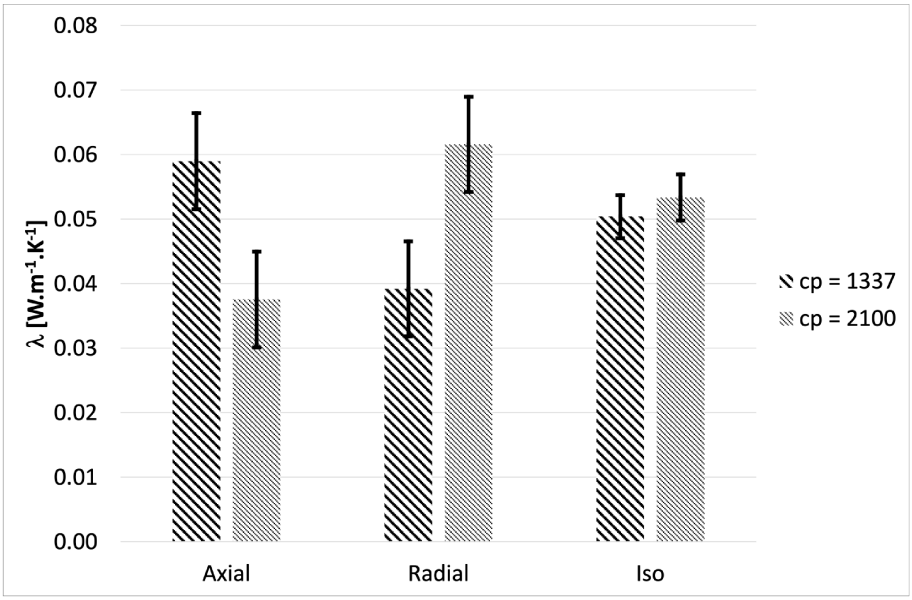

Figure 5: Thermal conductivities (λ_z and λ_r) estimated from anistropic model and λ_{HD} estimated from isotropic model as function of specific heat capacity c_p.

3.3 Light-earth biobased concrete

All samples of light-earth biobased concrete are first tested under steady-state with GHP. Results are plotted on Figure 6 and compared to literature data obtained by steady state methods (guarded hot plate or heat flowmeter) [36, 58-61]. As expected, we note that λ_{GHP} increases with density (or compacity) since earth is more conductive than hemp shiv. T-samples exhibit higher λ_{GHP} than P-samples. Because of alignment of elongated hemp shiv particles (see Figure 7), more interface thermal contact resistances are created, leading to low thermal conductivity of P-samples. For T-samples, particles are randomly set in the *xz*-plane (see Figure 7): heat conduction may also take place along the particles increasing thus the thermal conductivity. The thermal conductivity ratio between T and P-samples decreases slightly with density and ranges between 1.23 and 1.17 (see Figure 8). However, the ratio for samples T35r/P35r is slightly higher and equal to 1.29. These samples are made with a higher hemp fraction (resp.

lower earth slip fraction), for which particle rearrangement is expected to be different. Because of this influence of formulation and manufacturing process, a true comparison with literature data [36, 60, 62] is difficult, even if similar order of magnitude is observed.

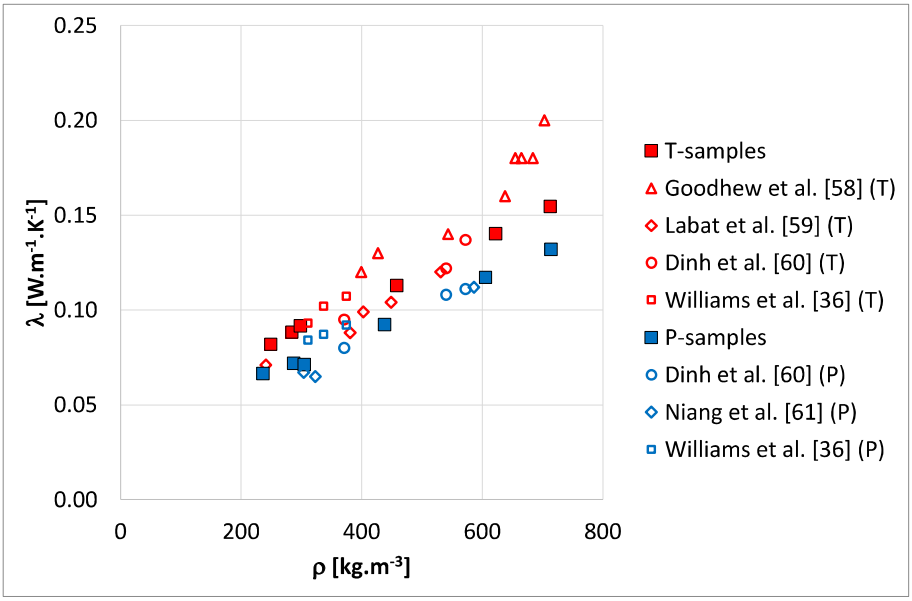

Figure 6: Comparison of thermal conductivity of light-earth biobased concrete P- and T-samples measured with guarded hot plate device (λ_{GHP}) with literature data.

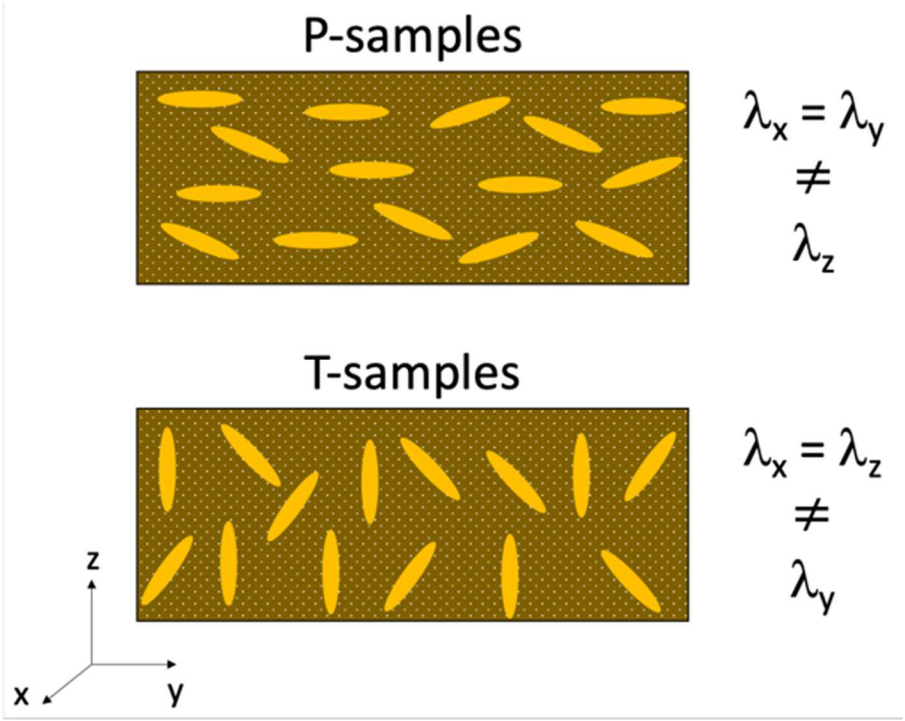

Figure 7: Schematic representation of hemp shiv particle orientation for P- and T-samples.

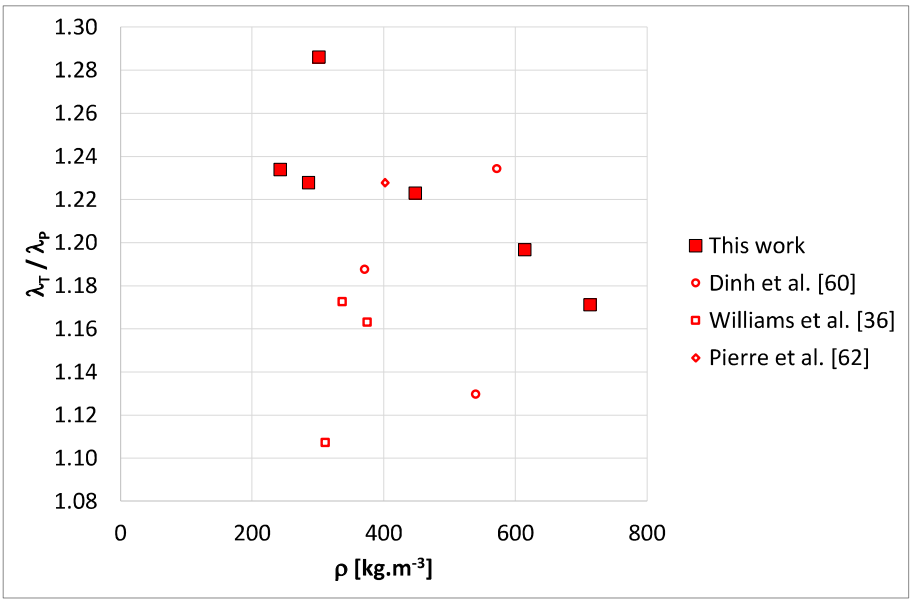

Figure 8: Thermal conductivity ratio between light-earth biobased concrete T and P-samples and comparison with literature data.

These results are then compared on Figure 9 with HD measurements performed with three sensors (6.403 mm, 9.868 mm, 14.61 mm) and analyzed with isotropic model. Since light-earth biobased concrete is a heterogeneous material at centimeter scale, measurements performed with sensor 6.403 mm show a different behavior and are not further analyzed in accordance with [18]. The measurements with the two other sensors are reliable, the standard deviation being always lower than 10 %. Similarly to WFI, λ_{HD} differs significantly from λ_{GHP}. The difference increases with density and may reach 80 %. Such differences are explained by heat transfer analysis in non-isotropic material. For instance, $\lambda_{GHP} = \lambda_z < \lambda_{x,y}$ for P-samples, while λ_{HD} can be viewed as a mean-like value between axial and radial thermal conductivities: $\lambda_{HD} = \sqrt{\lambda_z \lambda_{x,y}}$. Similar analysis prevails for T-samples. However, averaging thermal conductivities of each direction lead to similar values of λ_{HD} for T and P-samples (contrary to GHP measurements).

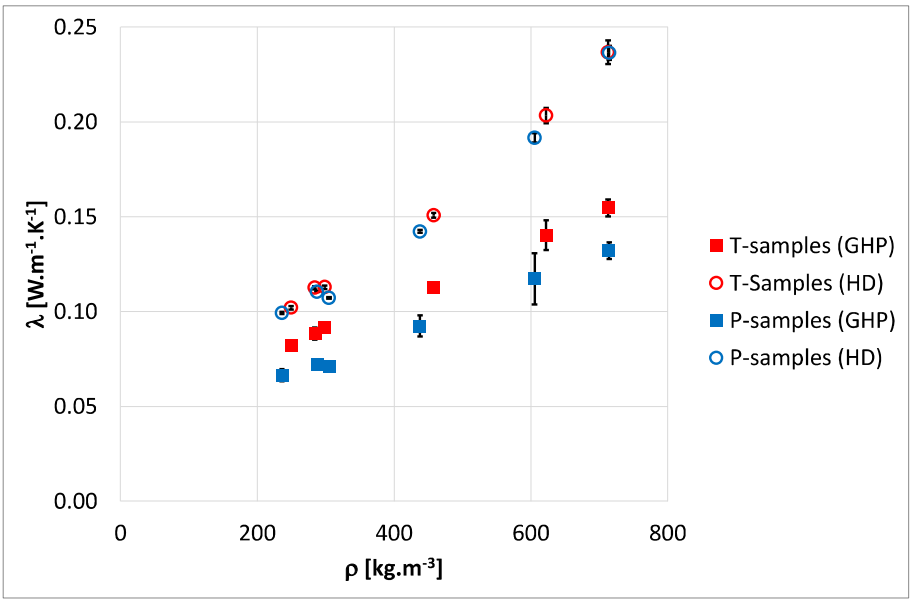

Figure 9: Thermal conductivity of light-earth biobased concrete P- and T-samples measured with guarded hot plate device (λ_{GHP}) and Hot Disk using isotropic model (λ_{HD}).

When using anisotropic model, the repeatability ranges from 2 to 30 % due to the influence of bound for estimation, while the reproducibility ranges from 5 to 30 % due to surface heterogeneity. When volumetric heat capacity ρc_p measured by DSC is used as input, λ_z is higher than λ_r and significantly higher than λ_{GHP} for all samples. Similar to WFI, such results were not expected, particularly for P-samples having elongated hemp shiv particles oriented perpendicularly to the sensor. As an alternative, we can adjust the volumetric heat capacity ρc_p of each sample so that $\lambda_z = \lambda_{GHP}$, and then calculate λ_r. Figure 10 shows the evolutions of the ratio λ_r/λ_z for P-samples. This ratio is much higher than unity, meaning that λ_r is higher than λ_z as expected. The ratio increases with density: macroporosity is reduced due to compression applied during manufacturing and to higher amount of earth: it increases conduction path in the in-plane direction and, thus, radial thermal conductivity. Nevertheless, the estimated ratios are higher to the ones predicted by homogenization modelling [63,64], limiting the validity of this approach. This limitation is confirmed when comparing axial thermal conductivity of T-samples $\lambda_z^{T-sample}$ with radial thermal conductivity of P-samples $\lambda_r^{P-sample}$. Whereas both

values should be equal according to ideal representation of Figure 7, results plotted in Figure 11 show that it is not the case. Finally, evaluating radial thermal conductivity by setting axial thermal conductivity to steady state measurement do not lead to consistent results for light-earth biobased concrete (contrary to wood fiber insulation which is more transverse isotropic).

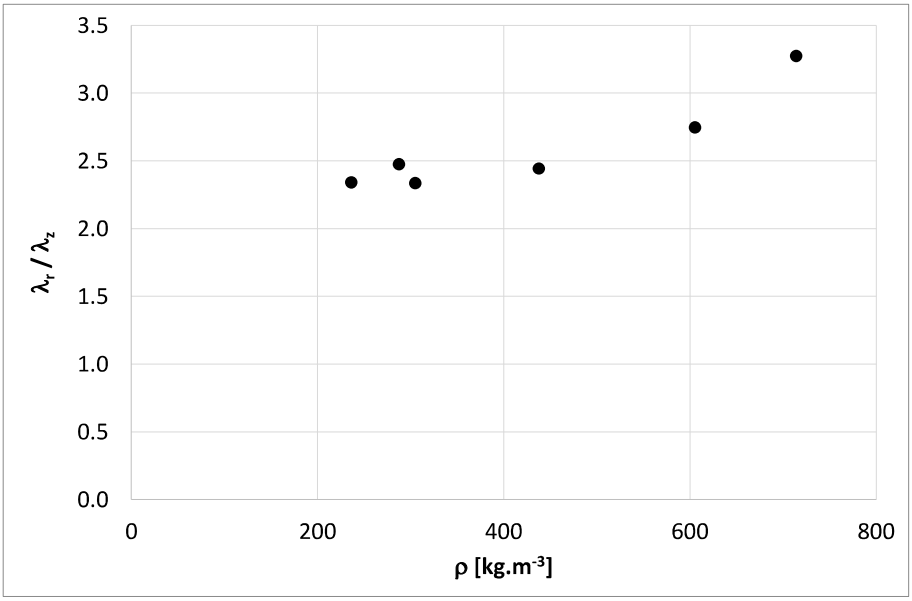

Figure 10: Thermal conductivity ratio λ_z/λ_r of P-samples estimated assuming that $\lambda_z = \lambda_{GHP}$.

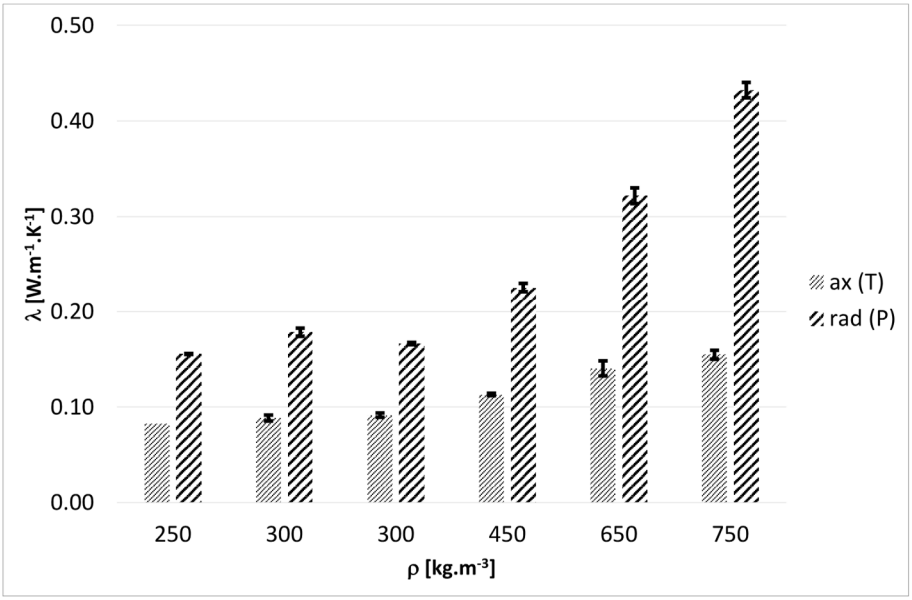

Figure 11: Comparison of axial thermal conductivity of T-samples $\lambda_z^{T-sample}$ with radial thermal conductivity of P-samples $\lambda_r^{P-sample}$. Both are estimated assuming that $\lambda_z = \lambda_{GHP}$.

4 Conclusions

This work aims to measure thermal conductivity of insulation building materials with Hot Disk device by applying transient plane source method and to compare the results with steady state measurements. The following main conclusions can be drawn:

- Thermal conductivity of isotropic conventional materials (PU, XPS, FG and AAC) can be accurately measured with Hot Disk, particularly by setting volumetric heat capacity ρc_p: reproducibility errors remain lower than 5 % and a good agreement with steady state measurement is found. Besides, neither estimation procedure, nor applied pressure, nor sensor size influence significantly the measurement.
- For non-isotropic materials, we first noted that reproducibility errors may reach 30 % due to an inhomogeneous and poor thermal contact between the sensor and the samples caused by heterogeneity of tested materials at centimeter scale and eventually by their compressive behavior. Second, analyzing the measurement with an isotropic model leads to an overestimation of thermal conductivity by at least 25% compared to Guarded Hot Plate measurements. Last, using anisotropic model to evaluate in-plane and through-plane thermal conductivities is not appropriate since the tested materials are not purely transverse isotropic and the results are very sensitive to volumetric heat capacity ρc_p. Alternatively, we suggest setting ρc_p so that though-plane thermal conductivity equals Guarded Hot Plate measurements, and then evaluating the anisotropy ratio of thermal conductivity. This approach works well for purely transverse isotropic materials (like wood fiber insulation), while it fails for more random material like light-earth biobased concretes.

Finally, this study has shown the difficulty to get an accurate estimation of thermal conductivity of heterogeneous biobased insulation building materials with Hot Disk. The device can be used

for internal comparative analysis (for instance, to evaluate the influence of factors like density), but the comparison of the results with literature data is not recommended. Nevertheless, further improvements are welcome since transient methods are expected to be less sensitive to moisture transfer than steady state methods when measuring thermal conductivity of moist samples.

5 Acknowledgement

This study is a part of the ECO-TERRA project (Development of light earth construction materials for efficient green buildings), with the support of ADEME, Fondation de France, Brittany and Normandy Regions and French Ministry of Education and Research.

6 References

[1] Jelle, B. P. (2011). Traditional, state-of-the-art and future thermal building insulation materials and solutions–Properties, requirements and possibilities. Energy and buildings, 43(10), 2549-2563.

[2] Schiavoni, S., Bianchi, F., & Asdrubali, F. (2016). Insulation materials for the building sector: A review and comparative analysis. Renewable and Sustainable Energy Reviews, 62, 988-1011.

[3] Aditya, L., Mahlia, T. M. I., Rismanchi, B., Ng, H. M., Hasan, M. H., Metselaar, H. S. C., ... & Aditiya, H. B. (2017). A review on insulation materials for energy conservation in buildings. Renewable and sustainable energy reviews, 73, 1352-1365.

[4] Abu-Jdayil, B., Mourad, A. H., Hittini, W., Hassan, M., & Hameedi, S. (2019). Traditional, state-of-the-art and renewable thermal building insulation materials: An overview. Construction and Building Materials, 214, 709-735.

[5] Jannot, Y., & Degiovanni, A. (2018). Thermal properties measurement of materials. ISTE Limited.

[6] Baldinelli, G., Bianchi, F., Gendelis, S., Jakovics, A., Morini, G. L., Falcioni, S., ... & Asdrubali, F. (2019). Thermal conductivity measurement of insulating innovative building materials by hot plate and heat flow meter devices: A Round Robin Test. International Journal of Thermal Sciences, 139, 25-35.

[7] Gustafsson, S. E. (1991). Transient plane source techniques for thermal conductivity and thermal diffusivity measurements of solid materials. Review of scientific instruments, 62(3), 797-804.

[8] ISO 22007-2. (2015). Plastics—Determination of Thermal Conductivity and Thermal Diffusivity—Part 2: Transient Plane Heat Source (Hot Disc) Method.

[9] Log, T., & Gustafsson, S. E. (1995). Transient plane source (TPS) technique for measuring thermal transport properties of building materials. Fire and materials, 19(1), 43-49.

[10] Campanale, M., & Moro, L. (2016). Thermal conductivity of moist autoclaved aerated concrete: Experimental comparison between heat flow method (HFM) and transient plane source technique (TPS). Transport in Porous Media, 113(2), 345-355.

[11] Trofimov, A. A., Atchley, J., Shrestha, S. S., Desjarlais, A. O., & Wang, H. (2020). Evaluation of measuring thermal conductivity of isotropic and anisotropic thermally insulating materials by transient plane source (Hot Disk) technique. Journal of Porous Materials, 27(6), 1791-1800.

[12] Almanza, O., Rodríguez-Pérez, M. A., & De Saja, J. A. (2004). Applicability of the transient plane source method to measure the thermal conductivity of low-density polyethylene foams. Journal of Polymer Science Part B: Polymer Physics, 42(7), 1226-1234.

[13] Al-Ajlan, S. A. (2006). Measurements of thermal properties of insulation materials by using transient plane source technique. Applied thermal engineering, 26(17-18), 2184-2191.

[14] Johansson, P., Adl-Zarrabi, B., & Hagentoft, C. E. (2012). Using transient plane source sensor for determination of thermal properties of vacuum insulation panels. Frontiers of Architectural Research, 1(4), 334-340.

[15] Coquard, R., Coment, E., Flasquin, G., & Baillis, D. (2013). Analysis of the hot-disk technique applied to low-density insulating materials. International journal of thermal sciences, 65, 242-253.

[16] Laskowski, J., Milow, B., & Ratke, L. (2016). Aerogel–aerogel composites for normal temperature range thermal insulations. Journal of Non-Crystalline Solids, 441, 42-48.

[17] Kerschbaumer, R. C., Stieger, S., Gschwandl, M., Hutterer, T., Fasching, M., Lechner, B., ... & Friesenbichler, W. (2019). Comparison of steady-state and transient thermal conductivity testing methods using different industrial rubber compounds. Polymer Testing, 80, 106121.

[18] Zheng, Q., Kaur, S., Dames, C., & Prasher, R. S. (2020). Analysis and improvement of the hot disk transient plane source method for low thermal conductivity materials. International Journal of Heat and Mass Transfer, 151, 119331.

[19] Bohac, V., Gustavsson, M. K., Kubicar, L., & Gustafsson, S. E. (2000). Parameter estimations for measurements of thermal transport properties with the hot disk thermal constants analyzer. Review of scientific instruments, 71(6), 2452-2455.

[20] He, Y. (2005). Rapid thermal conductivity measurement with a hot disk sensor: Part 1. Theoretical considerations. Thermochimica acta, 436(1-2), 122-129.

[21] Jannot, Y., & Acem, Z. (2007). A quadrupolar complete model of the hot disc. Measurement science and technology, 18(5), 1229.

[22] Li, Y., Shi, C., Liu, J., Liu, E., Shao, J., Chen, Z., ... & Hu, X. (2013). Improving the accuracy of the transient plane source method by correcting probe heat capacity and resistance influences. Measurement Science and Technology, 25(1), 015006.

[23] Zhang, H., Jin, Y., Gu, W., Li, Z. Y., & Tao, W. Q. (2013). A numerical study on the influence of insulating layer of the hot disk sensor on the thermal conductivity measuring accuracy. Progress in Computational Fluid Dynamics, an International Journal, 13(3-4), 191-201.

[24] Mihiretie, B. M., Cederkrantz, D., Rosén, A., Otterberg, H., Sundin, M., Gustafsson, S. E., & Karlsteen, M. (2017). Finite element modeling of the Hot Disc method. International Journal of Heat and Mass Transfer, 115, 216-223.

[25] Zhang, H., Li, Y. M., & Tao, W. Q. (2017). Theoretical accuracy of anisotropic thermal conductivity determined by transient plane source method. International Journal of Heat and Mass Transfer, 108, 1634-1644.

[26] Elkholy, A., Sadek, H., & Kempers, R. (2019). An improved transient plane source technique and methodology for measuring the thermal properties of anisotropic materials. International Journal of Thermal Sciences, 135, 362-374.

[27] Asdrubali, F., D'Alessandro, F., & Schiavoni, S. (2015). A review of unconventional sustainable building insulation materials. Sustainable Materials and Technologies, 4, 1-17.

[28] Amziane, S., & Sonebi, M. (2016). Overview on Biobased Building Material made with plant aggregate. RILEM Technical Letters, 1, 31-38.

[29] Laborel-Preneron, A., Aubert, J. E., Magniont, C., Tribout, C., & Bertron, A. (2016). Plant aggregates and fibers in earth construction materials: A review. Construction and Building Materials, 111, 719-734.

[30] Bouguerra, A., Laurent, J. P., Goual, M. S., & Queneudec, M. (1997). The measurement of the thermal conductivity of solid aggregates using the transient plane source technique. Journal of Physics D: Applied Physics, 30(20), 2900.

[31] de Bruijn, P., & Johansson, P. (2013). Moisture fixation and thermal properties of lime–hemp concrete. Construction and Building Materials, 47, 1235-1242.

[32] Gourlay, E., Glé, P., Marceau, S., Foy, C., & Moscardelli, S. (2017). Effect of water content on the acoustical and thermal properties of hemp concretes. Construction and Building Materials, 139, 513-523.

[33] ISO 12570. (2002). Hygrothermal performance of building materials and products–Determination of moisture content by drying at elevated temperature.

[34] Vinceslas, T., Colinart, T., Hamard, E., de Ménibus, A. H., Lecompte, T., & Lenormand, H. (2019). Light Earth Performances For Thermal Insulation:

Application To Earth–Hemp. In Earthen Dwellings and Structures (pp. 357-367). Springer, Singapore.

[35] Colinart, T., Vinceslas, T., Lenormand, H., De Menibus, A. H., Hamard, E., & Lecompte, T. (2020). Hygrothermal properties of light-earth building materials. Journal of Building Engineering, 29, 101134.

[36] Williams, J., Lawrence, M., & Walker, P. (2017). The influence of the casting process on the internal structure and physical properties of hemp-lime. Materials and Structures, 50(2), 108.

[37] Carré, P., & Le Gall, R. (1990). Définition et détermination des conductivités thermiques dans les structures multicouches CVR-balsa. Revue générale de thermique, 29(340), 211-215.

[38] Berger, J., Colinart, T., Loiola, B. R., & Orlande, H. R. (2020). Parameter estimation and model selection for water sorption in a wood fibre material. Wood Science and Technology, 54(6), 1423-1446.

[39] EN 12664. (2001). Thermal performance of building materials and products determination of thermal resistance by means of guarded hot plate and heat flow meter methods dry and moist products of medium and low thermal resistance.

[40] ISO 11357-4. (2003). Plastics-Differential Scanning Calorimetry (DSC)-Part 4: Determination of Specific Heat Capacity.

[41] Boháč, V., Gustavsson, M., Kubičár, Ľ., & Vretenár, V. (2003). Measurements of building materials by transient methods. In Proceedings of the Meeting of the Thermophysical Society-Working Group of the Slovak Physical Society, 53-66.

[42] Instruction Manual: Hot Disk Thermal Constants Analyzer, Hot Disk Inc., 1999

[43] Amaral, C., Vicente, R., Ferreira, V. M., & Silva, T. (2017). Polyurethane foams with microencapsulated phase change material: Comparative analysis of thermal conductivity characterization approaches. Energy and Buildings, 153, 392-402.

[44] Boumaza, T., & Redgrove, J. (2003). Use of the transient plane source technique for rapid multiple thermal property measurements. International journal of thermophysics, 24(2), 501-512.

[45] König, J., Petersen, R. R., Iversen, N., & Yue, Y. (2018). Suppressing the effect of cullet composition on the formation and properties of foamed glass. Ceramics International, 44(10), 11143-11150.

[46] Salmon, D. R., & Tye, R. P. (2010). An Inter-Comparison of Two Methods for Measuring the Thermal Conductivity of Low-Density Masonry Materials. In Thermal Conductivity 30: Thermal Expansion 18: Joint Conferences: August 29-September 2, 2009, Pittsburgh, Pennsylvania, USA.

[47] El Hachem, C., Ye, P., Abahri, K., & Bennacer, R. (2017). Fiber's hygromorphic effect on thermal conductivity of wooden fibrous insulation characterized by X-ray tomography. Construction and Building Materials, 150, 758-765.

[48] Labat, M., Woloszyn, M., Garnier, G., & Roux, J. J. (2015). Dynamic coupling between vapour and heat transfer in wall assemblies: Analysis of measurements achieved under real climate. Building and Environment, 87, 129-141.

[49] Slimani, Z., Trabelsi, A., Virgone, J., & Zanetti Freire, R. (2019). Study of the Hygrothermal Behavior of Wood Fiber Insulation Subjected to Non-Isothermal Loading. Applied Sciences, 9(11), 2359.

[50] Traoré, I. (2011). Transferts de chaleur et de masse dans les parois des bâtiments à ossature bois (Doctoral dissertation, Université Henri Poincaré-Nancy 1).

[51] Gobbé, C., Iserna, S., & Ladevie, B. (2004). Hot strip method: application to thermal characterisation of orthotropic media. International Journal of Thermal Sciences, 43(10), 951-958.

[52] Lux, J., Ahmadi, A., Gobbé, C., & Delisée, C. (2006). Macroscopic thermal properties of real fibrous materials: Volume averaging method and 3D image analysis. International Journal of Heat and Mass Transfer, 49(11-12), 1958-1973.

[53] Vololonirina, O., Coutand, M., & Perrin, B. (2014). Characterization of hygrothermal properties of wood-based products–Impact of moisture content and temperature. Construction and Building Materials, 63, 223-233.

[54] Marmoret, L., Humaish, H., Perwuelz, A., & Béji, H. (2016). Anisotropic structure of glass wool determined by air permeability and thermal conductivity measurements. Journal of Surface Engineered Materials and Advanced Technology, 6(02), 72.

[55] Louërat, M., Ayouz, M., & Perré, P. (2018). Heat and moisture diffusion in spruce and wood panels computed from 3-D morphologies using the Lattice Boltzmann method. International Journal of Thermal Sciences, 130, 471-483.

[56] https://www.soprema.fr/fr/product/isolation/toiture/toiture-en-pente/rampants/pavaflex-confort

[57] https://wufi.de

[58] Goodhew, S., Boutouil, M., Streiff, F., Le Guern, M., Carfrae, J., & Fox, M. (2021). Improving the thermal performance of earthen walls to satisfy current building regulations. Energy and Buildings, 240, 110873.

[59] Labat, M., Magniont, C., Oudhof, N., & Aubert, J. E. (2016). From the experimental characterization of the hygrothermal properties of straw-clay mixtures to the numerical assessment of their buffering potential. Building and Environment, 97, 69-81.

[60] Dinh, T. M., Magniont, C., Coutand, M., & Escadeillas, G. (2015). Hemp concrete using innovative pozzolanic binder. Academic Journal of Civil Engineering, 33(2), 265-270.

[61] Niang, I., Maalouf, C., Moussa, T., Bliard, C., Samin, E., Thomachot-Schneider, C., Lachi, M., Pron, H., Mai, T.H. & Gaye, S. (2018). Hygrothermal performance of various Typha–clay composite. Journal of Building Physics, 42(3), 316-335.

[62] Pierre, T., Colinart, T., & Glouannec, P. (2014). Measurement of thermal properties of biosourced building materials. International Journal of Thermophysics, 35(9-10), 1832-1852.

[63] Dartois, S., Mom, S., Dumontet, H., & Hamida, A. B. (2017). An iterative micromechanical modeling to estimate the thermal and mechanical properties of polydisperse composites with platy particles: Application to anisotropic hemp and lime concretes. Construction and Building Materials, 152, 661-671.

[64] Tran-Le, A. D., Nguyen, S. T., & Langlet, T. (2019). A novel anisotropic analytical model for effective thermal conductivity tensor of dry lime-hemp concrete with preferred spatial distributions. Energy and Buildings, 182, 75-87.